Petroleum Science 21 (2024) 1290–1304

Contents lists available at ScienceDirect

Petroleum Science

journal homepage: www.keaipublishing.com/en/journals/petroleum-science

Original Paper

Analysis and experimental study on resistance-increasing behavior of composite high efficiency autonomous inflow control device

Liang-Liang Dong [a, b, c, *], Yu-Lin Zhang [a, b]

[a] School of Mechatronic Engineering, Southwest Petroleum University, Chengdu, 610500, Sichuan, China
[b] State Key Laboratory of Oil and Gas Reservoir Geology and Exploitation, Southwest Petroleum University, Chengdu, 610500, Sichuan, China
[c] Oil and Gas Equipment Technology, Sharing and Service Platform of Sichuan Province, Chengdu, 610500, Sichuan, China

ARTICLE INFO

Article history:
Received 28 February 2023
Received in revised form
3 July 2023
Accepted 21 September 2023
Available online 23 September 2023

Edited by Jia-Jia Fei and Min Li

Keywords:
Water control
Flow separation
Flow resistance-increasing
AICD device
Simulation and experiment

ABSTRACT

Bottom water coning is the main reason to reduce the recovery of horizontal bottom water reservoir. By water coning, we mean the oil-water interface changes from a horizontal state to a mound-shaped cone and breaks through to the wellbore. Autonomous inflow control device (AICD) is an important instrument maintain normal production after bottom water coning, however, the resistance increasing ability of the swirl type AICD is insufficient at present, which seriously affects the water control effect. Aiming this problem, this paper designs a multi-stage resistance-increasing and composite type AICD. The separation mechanism of oil-water two phases in this structure, the resistance form of oil-water single phase and the resistance-increasing principle of water phase are analyzed. Establishing the dual-phase multi-stage separation and resistance-increasing model, and verified by measuring the throttling pressure drop and oil-water volume fraction of the AICD, it is found that the composite type AICD has the effect of ICD and AICD at the same time, which can balance the production rate of each well section at the initial stage of production, delay the occurrence of bottom water coning. In the middle and later stages of production, water-blocking can be effectively increased to achieve water control and stable production. After structural sensitivity analysis, the influence law of various structural parameters on the water control performance of composite AICD was obtained. The simulation calculation results show that, compared with the existing swirl type AICD, composite AICD has higher sensitivity to moisture content, the water phase throttling pressure drop is increased by 4.5 times on average. The composite AICD is suitable for the entire stage of horizontal well production.

1. Introduction

Horizontal wells can greatly increase oil well production and recovery factor (Toshev and Rakhimov, 2022; Jie et al., 2022), while bottom water coning will lead to premature water breakthrough in the horizontal section, reduce oil production, and even shut in well and shut down in severe cases (Mahmood and Guo, 2021; Chen et al., 2021). Water control devices are widely used in the field to alleviate the problem of production reduction caused by bottom water coning (Dikshit et al., 2020; Sabet et al., 2022). Various types of water control devices have been developed in the industry, including ICD (passive) and AICD (autonomous) (Cui et al., 2020). The ICD by generating friction pressure drop and local pressure drop, to inhibit the oil in high permeability sections of horizontal wells is being rapid production, balance the production profile, which can delay the occurrence of bottom water coning (Pinilla et al., 2022; Zhu et al., 2019; Prakasa et al., 2019; Al-Jumah et al., 2022). Once bottom water breaks through into the wellbore, ICD fails to effectively limit the production of water, thus losing its function (Zhang et al., 2021). AICD can increase resistance to water according to the increase of water content in the fluid, even if the bottom water breakthrough can maintain the production for a certain period of time (Zhang et al., 2019). However, the water restricting effect of current spiral-flow type AICD is still insufficient, resulting in short production cycle of water free or low water cut in horizontal wells, which severely limits the popularity and application of the technology.

* Corresponding author. School of Mechatronic Engineering, Southwest Petroleum University, Chengdu, 610500, Sichuan, China.
E-mail address: dll181@163.com (L.-L. Dong).

https://doi.org/10.1016/j.petsci.2023.09.018

To improve the water control performance of AICD, many experts and scholars have conducted in-depth research on the structure and principle of the water control device. Jia et al. (2021) proposed a steady-state characteristic mechanical representation model of floating disc AICD, compared and analyzed the water restricted effect under different fluid properties and structural parameters, and obtained the optimal matching relationship between the radius of floating disc and inlet channel radius. Yang et al. (2020) based on the principle of automatic phase separation proposed a spiral-flow type AICD, analyzed the sensitivity relationship between throttling pressure drop and fluid properties, and optimized the structure. Buwauqi et al. (2022) based on Paha's law and Bernoulli's principle proposed a guide tube, fluid with different viscosity will produce different pressure drop, which gives the water control device the independent identification function, for unnecessary fluids, it will actively close the channel, stop production. Wang et al. (2014) based on the principles of flow separation and swirling resistance-increasing, combined the Y-shaped flow channel and circular chamber, initially realized oil-water separation and increase resistance to water, analyzing the relationship between structural parameters and throttling pressure drop, completed the optimization of device structure. Langaas et al. (2019) tracked and analyzed the data of ICD and AICD integrated in Norwegian offshore Alvheim Oilfield, and found that the AICD layout is adopted for the well section near the overlying gas cap, and the ICD layout is adopted for other locations, which can maximize the productivity. At present, spiral-flow type AICD has been widely used in oil fields of China due to its stable and reliable operation without moving parts inside. But it can only increase resistance by single-stage spiral flow, the resistance-increasing ability is insufficient, which seriously limits the water restricted ability.

In this paper, a composite type inflow control device (Fig. 1) is proposed by Simonds et al. (2023) and Yao et al. (2023), in which each diverter block direct the flow, and narrow channel restrict the flow, with increase of the number of the block and channel, the restricting effect is stronger. A multi-stage separation and resistance-increasing model is established, throttling pressure drop and oil-water volume fraction are verified through experiments. Further studied the influence factors of water restricted effect, analyzed the sensitivity of structural parameters of device to pressure drop and volume fraction, and optimized the device structure.

2. Analysis on the mechanism of water control and oil stabilization of the model

2.1. Principle of fluid separation

The composite type inflow control device contains one inlet and outlet and 4 diverter blocks, the diverter block divides the flow area into 2 flow paths, each path provides varying flow drag. Therefore, oil and water are subject to different degrees of restriction.

When the fluid viscosity is determined, frictional drag is proportional to the length of the flow channel. Take one diverter block area as an example, the frictional drag is shown in Fig. 2. Obviously, the blue path is longer than the red path, the fluid will suffer greater frictional drag in the blue path. The friction pressure drop is calculated as follows (Xu et al., 2019):

$$\Delta P_{\mathrm{f}} = \lambda \frac{l\rho\bar{v}^2}{2d} \tag{1}$$

where λ is the friction factor, l is the length of the flow path, ρ is the fluid density, $\bar{v}$ is the time-averaged velocity, and d is the equivalent diameter of the flow channel.

Oil as low-density and high-viscosity fluid, is mainly affected by frictional drag. When oil flow in the composite AICD device, it will pass through the upper and lower flow channels of the diverter block. However, due to the inconsistent frictional drag between the upper and lower flow channels, the flow rate of the oil will be slowed down in the flow channel (blue path) with high frictional drag, while the flow rate in the other flow channel (red path) with low frictional drag is faster, causing subsequent oil to choose the flow channel with low frictional drag.

Water as high-density and low-viscosity fluid, is mainly affected by differential pressure drag. When water flow in the composite AICD device, it also passes through the upper and lower flow channels of the diverter block. However, the frictional drag of water in both channels is very small, and the impact of frictional drag on water can be ignored. Therefore, the water flow rate in the upper and lower flow channels is consistent. However, its flow is affected by inertial forces, making it difficult to change the direction of flow. Without obstacles, it will maintain a straight flow, and when encountering obstacles, it will flow along the shape of the obstacle. When water passes through the first diverter block, the flow rate is evenly divided into the upper and lower flow channels of the

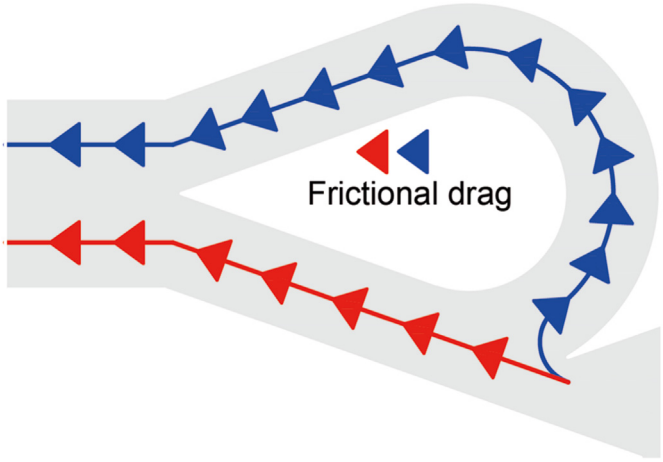

Fig. 2. Schematic diagram of friction drag.

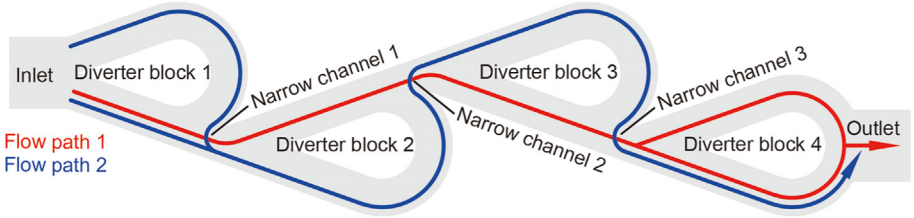

Fig. 1. Flow channel model of the composite water control device.

diverter block. When passing through the second diverter block, due to the lower flow channel of the second diverter block being tangent to the inflow direction, the water is affected by inertial forces, and most of the water flows in the original flow direction, causing most of the water to be distributed in the lower flow channel of the second guide block, while a small amount of water is distributed in the upper flow channel. Therefore, the tangential flow path (blue path) becomes the main flow path for water.

2.2. Principle of differential pressure drag stratum

Differential pressure drag is due to fluid create pressure drop in the direction of flow, this differential pressure can be created in front of and behind the obstacle, and also be created in the local position where the flow channel area and shape change. Therefore, the differential pressure drag can further be classified as the vortex drag and the local differential pressure drag.

(1) Vortex drag

When viscous fluid flows through the diverter block as shown in Fig. 1, it creates frictional drag in the tangential direction of the block surface, also creates flow pressure in the direction normal to the block surface. The pressure drop is calculated as follows:

$$\Delta P_{\mathrm{r}} = \int_A (P\cos\theta + \tau_\omega \sin\theta)\mathrm{d}A \tag{2}$$

where $P\cos\theta$ is the component of the diverter block surface pressure P in the flow direction, $\tau_\omega \sin\theta$ is the component of the diverter block surface frictional drag τ_ω in the flow direction, A is the lateral area of the diverter block, θ is the angle between the pressure P and the flow direction.

(2) Local differential pressure drag

There is a narrow channel between two diverter block areas, the flow rate changes suddenly as fluid passes through the location (Liu and Liang, 2022), then create a pressure drop before and after this position, forming flow drag:

$$\Delta P_{\mathrm{j}} = G^2\overline{\sigma_{\mathrm{e}}}(1-\overline{\sigma_{\mathrm{e}}})v_{\mathrm{f}} \tag{3}$$

where G is the mass flow rate, kg/(m^2 • s); $\overline{\sigma_{\mathrm{e}}}$ is the average expansion area ratio; v_{f} is the specific volume of the fluid, m^3/ kg.

2.3. Drag calculation equation

2.3.1. Frictional drag

Frictional drag has little effect in the low viscosity fluids, but in high viscosity fluids, it becomes dominant. The frictional drag for oil in this model can be expressed as:

$$\Delta P_{\mathrm{fo}} = \lambda\frac{l\rho\overline{v}^2}{2d} \tag{4}$$

2.3.2. Vortex drag

When water flows through the diverter block, due to the low viscosity, differential pressure drag becomes dominant. The vortex drag can be expressed as:

$$\Delta P_{\mathrm{r}} = \int_A P\cos\theta\mathrm{d}A \tag{5}$$

According to the drag coefficient $C_D = \frac{\Delta P_{\mathrm{r}}}{1/2\rho V^2 D}$ and the pressure coefficient (Huang et al., 2022) $C_P = \frac{P}{1/2\rho V^2}$, by changing the calculation equation of the drag coefficient C_D, the vortex drag equation related to the drag coefficient C_D can be obtained:

$$\Delta P_{\mathrm{r}} = C_D\frac{\rho V^2 D}{2} \tag{6}$$

where ρ is the fluid density, V is the average velocity of the fluid, and D is the wetted circumference of the diverter block.

The formula for calculating the area of the vortex at the tail of a two-dimensional square pier is:

$$S_{\mathrm{dz}} = k_0 D L_{\mathrm{dz}}, \tag{7}$$

The length L_{dz} of the vortex area is related to the fluid velocity V, the coefficient k_1 and the gravitational acceleration g:

$$L_{\mathrm{dz}} = k_1\frac{V^2}{2g} \tag{8}$$

Combining Eqs. (7) and (8) and bringing them into Eq. (6), the vortex drag equation related to the area of the tail vortex is obtained (where $k = \frac{C_D}{k_0 k_1}$, k_0 is the coefficient):

$$\Delta P_{\mathrm{r}} = k\rho g S_{\mathrm{dz}} \tag{9}$$

Therefore, the vortex drag equation of water is:

$$\Delta P_{\mathrm{rw}} = k\rho g S_{\mathrm{dz}} \tag{10}$$

Since water will be subjected to vortex drag in the four diverter block areas in this model, these drags can be superimposed, therefore, the total vortex drag for water is:

$$\Delta P_{\mathrm{rW}} = \Delta P_{\mathrm{rw1}} + \Delta P_{\mathrm{rw2}} + \cdots + \Delta P_{\mathrm{rw}i}\ ,\ i = 1,2,3,4 \tag{11}$$

2.3.3. Local differential pressure drag

When oil flows through a narrow channel, the flow velocity will decrease and a local pressure drop will be created before and after the position, so the local differential pressure drag of oil can refer to Eq. (3):

$$\Delta P_{\mathrm{jo}} = G_{\mathrm{o}}{}^2\overline{\sigma_{\mathrm{e}}}(1-\overline{\sigma_{\mathrm{e}}})v_{\mathrm{fo}} \tag{12}$$

The model has 3 narrow channels that can create differential pressure drag and these drags can be superimposed, so the total local differential pressure drag of oil is:

$$\Delta P_{\mathrm{jO}} = \Delta P_{\mathrm{jo1}} + \Delta P_{\mathrm{jo2}} + \Delta P_{\mathrm{jo3}} \tag{13}$$

When water passes through this position, it will also be affected by local difference pressure drag:

$$\Delta P_{\mathrm{jw}} = G_{\mathrm{w}}{}^2\overline{\sigma_{\mathrm{e}}}(1-\overline{\sigma_{\mathrm{e}}})v_{\mathrm{fw}} \tag{14}$$

Similarly, it can be known that the total local differential pressure drag of water is:

$$\Delta P_{\mathrm{jW}} = \Delta P_{\mathrm{jw1}} + \Delta P_{\mathrm{jw2}} + \Delta P_{\mathrm{jw3}} \tag{15}$$

In conclusion, the total drag to oil and water in this model is:

$$\begin{cases} \Delta P_{\mathrm{O}} = \Delta P_{\mathrm{fo}} + \Delta P_{\mathrm{jO}} \\ \Delta P_{\mathrm{W}} = \Delta P_{\mathrm{rW}} + \Delta P_{\mathrm{jW}} \end{cases} \tag{16}$$

Through the above drag equation, the flow field and differential

pressure drag distribution of oil and water in this model can be obtained, as shown in Fig. 3.

2.4. Flow field governing equations

2.4.1. Mass and momentum conservation equations

Mass conservation equation in differential form (continuity equation):

$$\frac{\partial \rho}{\partial t}+\nabla(\rho V)=0 \tag{17}$$

Momentum conservation equation in differential form (N–S equation):

$$\begin{cases}\dfrac{\partial(\rho u)}{\partial t}+\nabla\cdot(\rho u V)=-\dfrac{\partial P}{\partial x}+\dfrac{\partial \tau_{xx}}{\partial x}+\dfrac{\partial \tau_{yx}}{\partial y}+\dfrac{\partial \tau_{zx}}{\partial z}+\rho f_x\\ \dfrac{\partial(\rho v)}{\partial t}+\nabla\cdot(\rho v V)=-\dfrac{\partial P}{\partial y}+\dfrac{\partial \tau_{xy}}{\partial x}+\dfrac{\partial \tau_{yy}}{\partial y}+\dfrac{\partial \tau_{zy}}{\partial z}+\rho f_y\\ \dfrac{\partial(\rho w)}{\partial t}+\nabla\cdot(\rho w V)=-\dfrac{\partial P}{\partial z}+\dfrac{\partial \tau_{xz}}{\partial x}+\dfrac{\partial \tau_{yz}}{\partial y}+\dfrac{\partial \tau_{zz}}{\partial z}+\rho f_z\end{cases} \tag{18}$$

The above equations are combined to form the basic governing equations of the flow field, where ρ is the fluid density, u, v, and w are the velocities in the x, y, and z directions, V is the velocity scalar, P is the pressure distribution on the surface of the fluid micelle, τ_{xx} is the normal stress on the surface of the fluid micelle, and τ_{xy} is Shear stress, f_x, f_y, f_z are the body forces in the x, y, and z directions.

2.5. Conservation equation for two-phase flow field

The normal stress on the surface of the oil micelle is much smaller than the shear stress, so the influence of the shear stress on the flow is mainly considered; The shear stress on the surface of the water micelle is much smaller than the normal stress, so the influence of the normal stress on the flow is mainly considered. The body force f of the fluid micelle is only gravity, so the mass and momentum conservation equations of the oil-water two-phase flow field are (time-averaged processing):

$$\begin{cases}\dfrac{\partial \overline{\rho}}{\partial t}+\nabla(\overline{\rho}\overline{V})=0\\ \overline{\rho}\left(\dfrac{D\overline{u}}{Dt}+\dfrac{D\overline{v}}{Dt}+\dfrac{D\overline{w}}{Dt}\right)=F+\overline{\rho}^2 Q g\end{cases} \tag{19}$$

The above equation is also a governing equation for oil-water two-phase flow. The left side of the second equation in the above formula is the time-average velocity change rate, that is, the form of the derivative of matter, and the right side is the total surface force and volume force of the fluid micelle. Where F is the total surface force, including normal stress and shear stress; $\overline{\rho}$ is the average density, Q is the total volume of the fluid, and g is the acceleration of gravity.

2.6. Volume fraction equation for two-phase flow field

Oil and water are immiscible with each other and there is a clear interface between the phases, and the flow rule conforms to the VOF multiphase flow model. Therefore, the calculation equation of the volume fraction of oil and water two phases is:

$$\frac{\alpha_q^{n+1}\rho_q^{n+1}-\alpha_q^n\rho_q^n}{\Delta t}V+\sum_f\left(\rho_q U_f^n \alpha_{q,f}^n\right)=\left[\sum_{p=1}^{n}\left(\dot{m}_{pq}-\dot{m}_{qp}\right)+S_{\alpha q}\right]V \tag{20}$$

Where q and p respectively represent the phase of the fluid, if q is water, then p is oil; α_q^{n+1} and α_q^n are the unit values of the q-phase volume fraction at time steps $n+1$ and n, respectively; ρ_q^{n+1} and ρ_q^n are the unit values of the q-phase density at time steps $n+1$ and n, respectively; V is the unit volume; U_f is the volume flow; $\alpha_{q,f}$ is the face value of the volume fraction of the q phase; $\dot{m}_{pq}$ is the mass transfer from p phase to q phase, $\dot{m}_{qp}$ is the mass transfer from q phase to p phase; $S_{\alpha q}$ is the quality source item, which is 0 by default; $n+1$ represents the index of the current time step, and n represents the index of the previous time step.

3. Simulation model and experimental verification of separation resistance-increasing performance

3.1. Geometric modeling and meshing

The geometric model and object of the composite type AICD is shown in Fig. 4, and the flow channel structure composed of four diverter block areas. In the early stage of production, the high proportion of oil is mainly affected by the frictional drag of the device, which can delay the bottom water coning in the high permeability well section. After water breakthrough in production, water affected by the differential pressure drag of the device and increases with the increase of water content, so as to achieve water control and stable production.

The fluid region of the composite type AICD is extracted and meshed, as shown in Fig. 5, the global hexahedral mesh is used, and the local position is not refined due to the uniform distribution of the mesh, the grid independence verification is carried out, and the most suitable scheme is selected by calculating the pure water throttling pressure drop of the above model under different grid numbers. The results are shown in Table 1.

From the tabular data, it can be concluded that as the number of grids increases, the pressure drop first increases and then decreases and tends to stabilize, the error rates between adjacent schemes are 26.3%, 19%, 2.3%, and 0.06% (error rate: $\eta=\frac{P_2-P_1}{P_2}\%$), it can be seen that the error rate between scheme 4 and scheme 5 is the minimum, so the number of grids in scheme 4 is more reasonable.

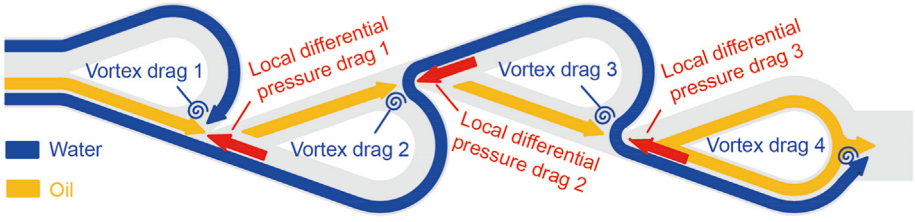

Fig. 3. Schematic diagram of model differential pressure drag.

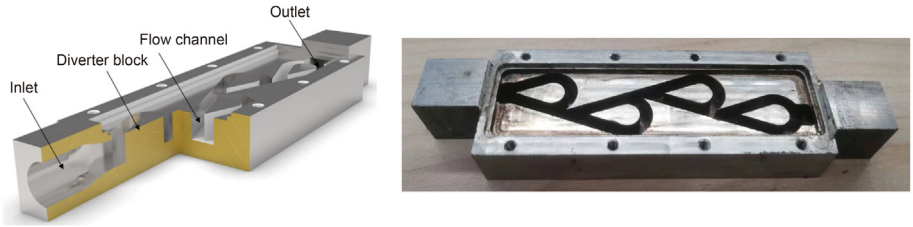

Fig. 4. Geometric model and object of composite type AICD.

Fig. 5. Fluid region meshing of composite type AICD.

Table 1
Mesh independence verification results.

Name	Grid size, mm	Number of grids	Pressure drop, Pa
Scheme 1	2	616	12896
Scheme 2	1	1698	17496
Scheme 3	0.5	14226	21596
Scheme 4	0.3	65010	21113
Scheme 5	0.2	223515	21100

3.2. Simulation analysis of resistance-increasing performance

The simulation analysis will be carried out from the throttling pressure drop of the oil, gasoline and water single phase, and comprehensively review the water control performance of the device. Simulation calculation parameters are shown in Table 2.

(1) Throttling pressure drop of single phase

Calculate the throttling pressure drop for oil, gasoline and water in turn, and the results are shown in Table 3.

(2) Volume fraction ratio of oil-water two-phase

To accurately calculate the volume fraction ratio of oil and water, the simulation calculation model shown in Fig. 6(a), (b) and (c) is proposed.

The model in Fig. 6(a) is a tee structure, the grey area is full of fluid, there are two outlets in the model with outlet2 attached to a composite type AICD. Outlet1 and outlet2 have a same size of flowing cross-section in Fig. 6(a), whereas in Fig. 6(b) and (c), the outlet1 flowing cross-section was reduced from original by 1/3 and 2/3, respectively. In the right figure of Fig. 6(a), oil and water flow in at a volume fraction ratio of 1:1, after a period of time, volume fraction of outlet2 oil increased to 93% and water decreased to 1%, oil-water volume fraction ratio is 9.3, this shows that the composite type AICD has a very significant water restricted effect when outlet1 have a same size with outlet2. In fact, although oil-water volume fraction ratio of outlet2 is large, the flow drag of outlet1 is much smaller than outlet2, this cause most of oil and water to flow out of outlet1, only a small part of the oil and water flow from outlet2. As the flowing section of outlet1 decreases, the flow pressure of outlet1 will increase, at the same time, the pressure of the AICD inlet will increase accordingly. It can be seen from right figure of Fig. 6(b)–(c) that with the decrease of the flowing section of outlet1, the oil-water volume fraction ratio of outlet2 is also decrease. In the right figure of Fig. 6(b) that after the flowing section of outlet1 is reduced by one third, the oil-water volume fraction ratio of outlet2 decreases to 3.75; In the right figure of Fig. 6(c), after the flowing section of outlet1 is reduced by two-thirds, the oil-water volume fraction ratio of outlet2 decreases to 2.

From the above conclusion, the pressure of the AICD inlet will increase with the decrease of outlet1 flowing section, this led to the decrease of AICD water restricted effect. we can infer that the water restricted effect provided by the composite type AICD is different when it working in different horizontal well section. According to the pressure of each well section, reasonable distributed the number of the AICD, to achieve the best water restricted effect.

Table 2
Simulation calculation parameters.

Fluids	Viscosity, cp	Density, kg/m^3
Oil	100	850
Gasoline	0.76	750
Water	1	1000

3.3. Experimental verification

Fig. 7(a) is a schematic diagram of the experimental setup, which can independently complete the pressure drop test and oil-water volume fraction test. As shown in the figure, close the switches 2 of T-joint A and switches 4 of T-joint B, and open the switches 1 and 3, to complete the oil pressure drop test; Close the switches 1 and 4, and open the switches 2 and 3, it complete the water pressure drop test. Open all the switches of T-joint A and T-joint B, and adjust switch 4 to change the flowing section of the flow channel, the fluids at the outlet beakers would be measured for oil and water volumes after standing for stratification complete the oil-water volume fraction test. Fig. 7(b) is the physical connection set up diagram, and Fig. 8 depicts the flow routes of oil and water during pressure drop testing.

Table 3
Simulation data of throttling pressure drop for oil, gasoline and water.

Water		Gasoline		Oil	
Flow rate, L/min	Pressure drop, Pa	Flow rate, L/min	Pressure drop, Pa	Flow rate, L/min	Pressure drop, Pa
1.8	6689	1.8	5513	1.8	11527
2.4	15651	2.4	10496	2.4	16117
4.8	53967	4.8	30497	4.8	36086
6	69889	6	49710	6	55090
7.2	92344	7.2	71837	7.2	79088
7.8	107100	7.8	85174	7.8	96301
8.4	128581	8.4	98555	8.4	108595
9	148035	9	123665	9	118205
9.6	172211	9.6	149326	9.6	128901
10.2	196008	10.2	175692	10.2	147349
10.8	225835	10.8	191701	10.8	162281
11.4	242243	11.4	212323	11.4	175029

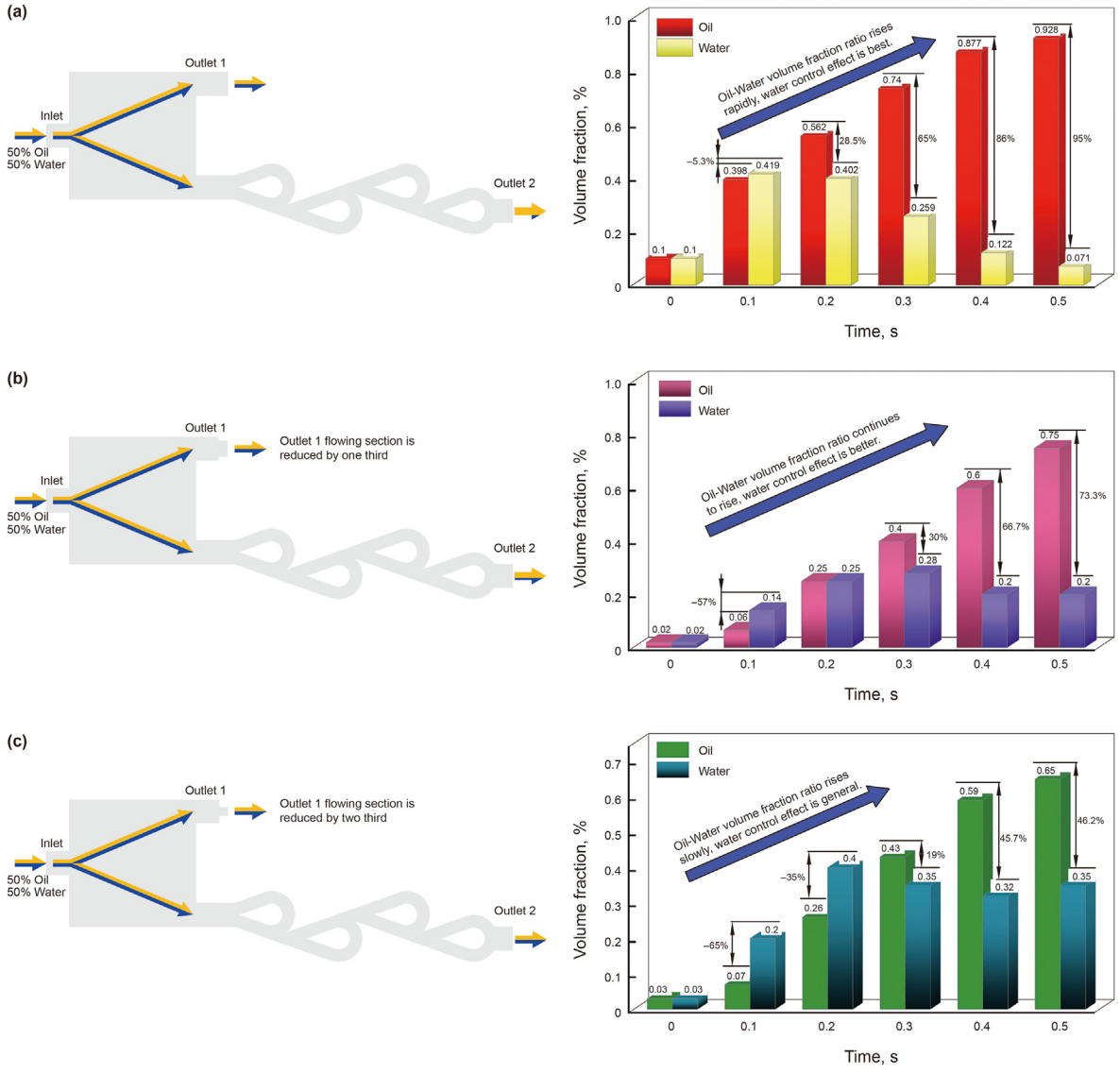

Fig. 6. Simulation model and calculation results of oil-water volume fraction. (**a**) Simulation model 1 and calculation results of oil-water volume fraction. (**b**) Simulation model 2 and calculation results of oil-water volume fraction. (**c**) Simulation model 3 and calculation results of oil-water volume fraction.

(1) Throttling pressure drop experiment

This experiment will measure the pressure drop of water (industrial distilled water), gasoline and oil (petroleum, viscosity is 98 cp) respectively, experimental materials and some measuring instruments are shown in Fig. 9.

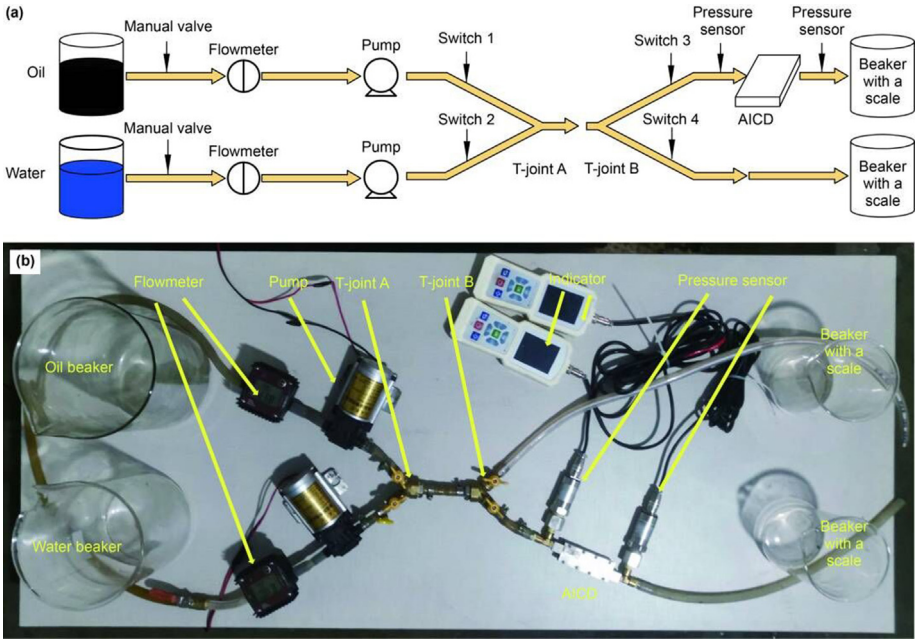

Fig. 7. Connection diagram of experimental device. (**a**) Schematic diagram of the experimental setup. (**b**) Physical connection diagram.

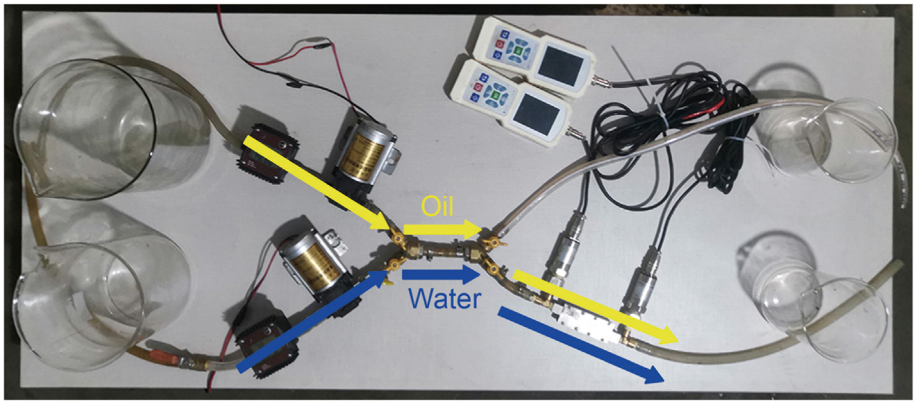

Fig. 8. The flow route of oil and water in the experimental device.

Measure the pressure drop of water, gasoline and oil in turn according to the above operation sequence and method. Adjust the manual valve once for each experiment to obtain the pressure drop under different flow rates. The pressure drop experimental data of water, gasoline and oil are shown in Table 4, comparison of pressure drop experimental data and simulation data are shown in Fig. 10.

As can be seen from Fig. 10, with the increase of flow rate, the pressure drop of water is the largest, followed by gasoline, and the pressure drop of oil is the smallest. When the flow rate is low, the pressure drop of oil is greater than that of water and gasoline. This is because the differential pressure drag of water and gasoline at low flow rate is smaller, and oil is always subject to greater friction drag. The density and viscosity of gasoline are very close to that of water, so the pressure drop changes rule are basically the same, because of its smaller density, gasoline suffers less inertial force, therefore, the pressure drop is less than that of water.

The experimental pressure drop data are universally greater than the simulation data, this is because there is a slight difference between the pressure measuring position of the experimental device and those of the simulation model. The simulation model directly measures the AICD's inlet and outlet pressure, but the installation of pressure gauge has to be considered for the experimental device, and tee joints need to be respectively connected at the inlet and outlet of AICD device. The diameter of the tee joint is smaller than the inlet diameter of AICD device, so the fluid at the tee joint will be affected by resistance, resulting in pressure rise. This error can be reduced through subsequent improvement of the model.

(2) Volume fraction ratio experiment

Open all valves and switches of the experimental device, then close the switch 4 by one third as shown in Fig. 11(a). Turn on the water pump and oil pump at the same time, and adjust the manual valve until the flow values of water and oil are equal. During this period, the oil and water from the two outlets are temporarily collected in the same beaker. After the flow of oil and water is adjusted to be the same, the oil and water from the two outlets are collected into two different beakers. After the experiment is completed, clean the pipe and reduce the switch 4 of T-joint B by

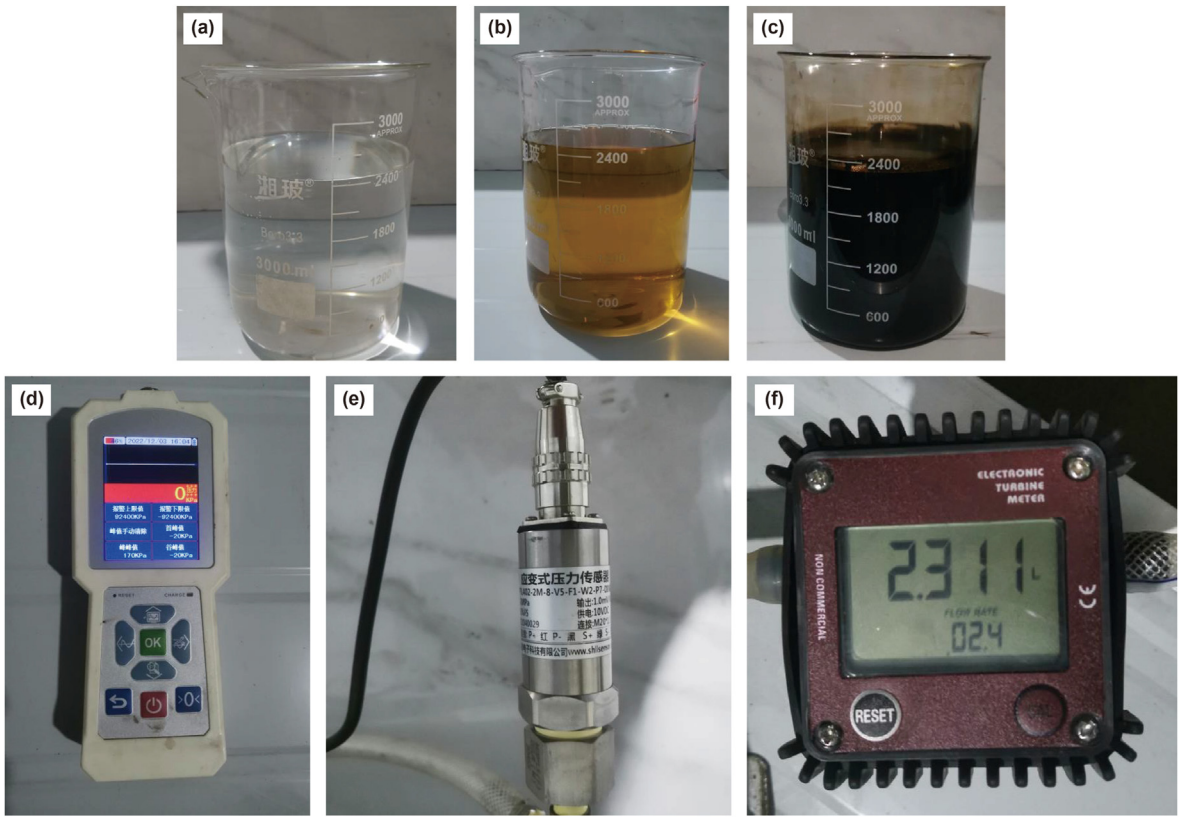

Fig. 9. Experimental materials and measuring instruments. (**a**) Water. (**b**) Gasoline. (**c**) Oil (petroleum). (**d**) Digital pressure gauge. (**e**) Pressure sensor. (**f**) Digital flowmeter.

Table 4
Experimental data of throttling pressure drop for oil, gasoline and water.

Water		Gasoline		Oil	
Flow rate, L/min	Pressure drop, Pa	Flow rate, L/min	Pressure drop, Pa	Flow rate, L/min	Pressure drop, Pa
1.8	10000	1.8	10000	1.8	20000
2.4	20000	2.4	20000	2.4	30000
4.8	60000	4.8	40000	4.8	60000
6	80000	6	60000	6	80000
7.2	110000	7.2	90000	7.2	100000
7.8	130000	7.8	110000	7.8	120000
8.4	150000	8.4	130000	8.4	130000
9	180000	9	150000	9	140000
9.6	200000	9.6	170000	9.6	150000
10.2	230000	10.2	210000	10.2	160000
10.8	250000	10.8	230000	10.8	180000
11.4	270000	11.4	250000	11.4	200000

two-thirds, then repeat the experiment. The volume of gasoline and water is shown in Fig. 11(c)–(d), the volume of oil and water is shown in Fig. 11(e)–(f).

As can be seen from Fig. 11(c)–(d), no matter how the opening of switch 4 changes, the volume of gasoline and water flowing from the AICD outlet is always equal. This shows that the composite type AICD cannot increase gasoline production. As shown in Fig. 11(e)–(f), when switch 4 is reduced by one third, the volume of oil flowing from the AICD outlet is three times that of water, but the total volume of oil and water is small. As the opening of switch 4 continues to decrease, the volume fraction ratio of oil and water flowing out of AICD outlet is also decreasing. This also shows that with the increase of AICD inlet pressure, its water restricted effect decreases.

Comparing the experimental data of oil-water volume fraction with the simulation data, it can be found that, when switch 4 is reduced by one third, the experimental value of volume fraction ratio is 3, and simulation value of volume fraction ratio is 3.75; When switch 4 is reduced by two third, the experimental value of volume fraction ratio is 2, and simulation value of volume fraction ratio is 1.9, the experimental data are more agree with the simulation data. This experiment confirms the validity of the simulation calculation, and also shows that the composite type AICD has good water restricted ability.

4. Sensitivity analysis of structural parameters of water control device

To study the water-controlling and oil-stabilizing performance of the device, it is necessary to conduct a sensitivity analysis on the structural parameters of the model to further improve the water-controlling capability of the device. The specific structural

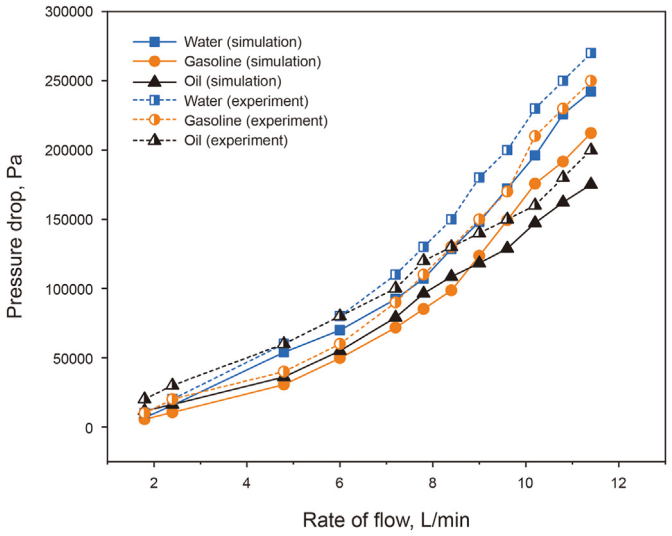

Fig. 10. Pressure drop data of experiment and simulation.

parameters of the model are shown in Table 5. Schematic diagram of structural parameters is shown in Fig. 12.

4.1. Outlet position

For this study, five outlet positions will be investigated: upside, upside middle, middle, bottom middle and bottom. Fig. 13 shows the velocity contours and pressure contours of oil and water (the pressure drop laws and flow paths of each optimization model are similar, so only part of the contours are listed). It can be seen from the pressure contours that the differential pressure of oil before and after each narrow channel is much smaller than that of water except narrow channel 1, indicating that the local differential pressure drag of oil is smaller. Because when the water flows through the diverter block 2 and 3, the water flow rate on both sides of the diverter block is different, water flow rate on the side of long flow path is large, when this water converges at the narrow channel 2 and 3, due to the change of the flow direction, it will produce a large vortex, which will produce a large pressure drop before and after the narrow channel 2 and 3. At the same time, it

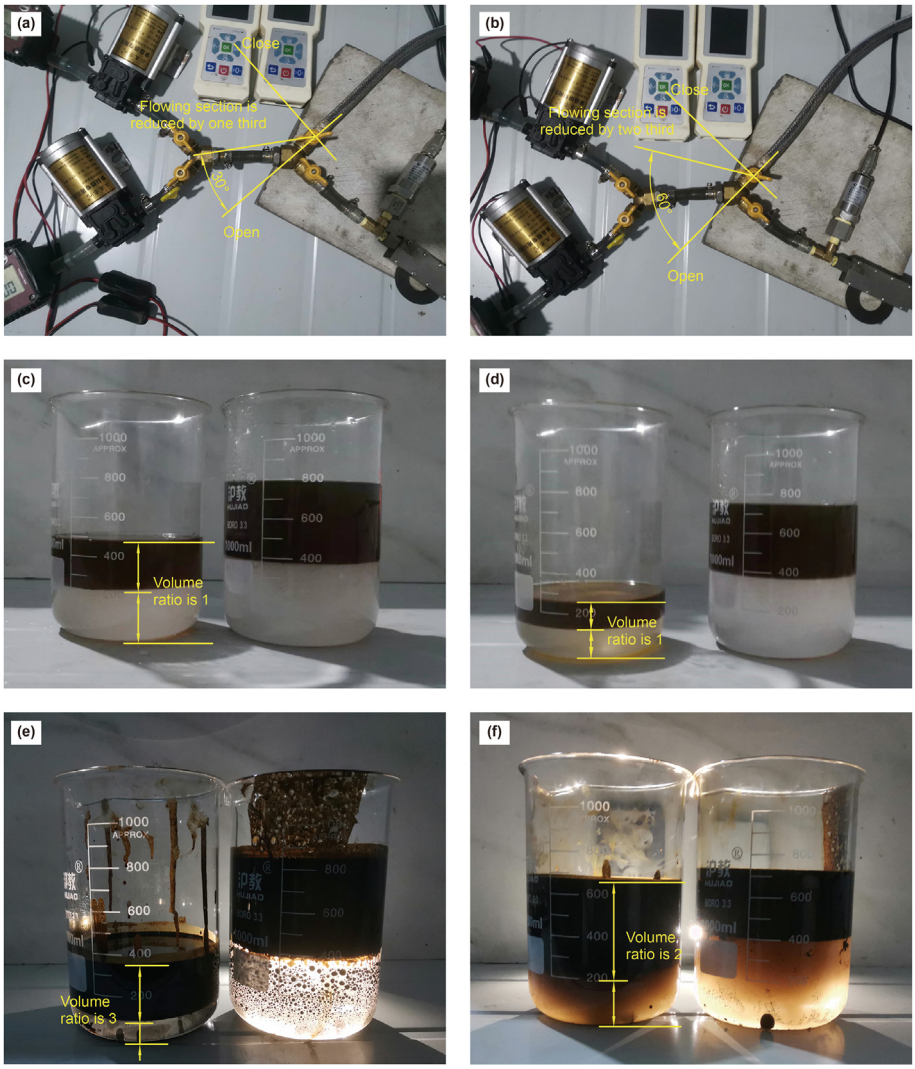

Fig. 11. Experimental process and results. (**a**) Switch 4 turns off one third. (**b**) Switch 4 turns off two third. (**c**) Volume of gasoline and water corresponds to Fig. 11(a) (left beaker corresponds to the outlet of AICD). (**d**) Volume of gasoline and water corresponds to Fig. (b) (left beaker corresponds to the outlet of AICD). (**e**) Volume of oil and water corresponds to Fig. 11(a) (left beaker corresponds to the outlet of AICD). (**f**) Volume of oil and water corresponds to Fig. 11(b) (left beaker corresponds to the outlet of AICD).

Table 5
Structural parameters of composite type AICD.

Outlet position	Number of diverter blocks	Diverter block cone angle, °	Flow channel width, mm
Upside, upside middle, middle, bottom middle, bottom	4	39	3
Middle	2, 3, 4, 5, 6	39	3
Middle	4	34, 36, 39, 44, 50	3
Middle	4	39	2, 2.5, 3, 3.5, 4

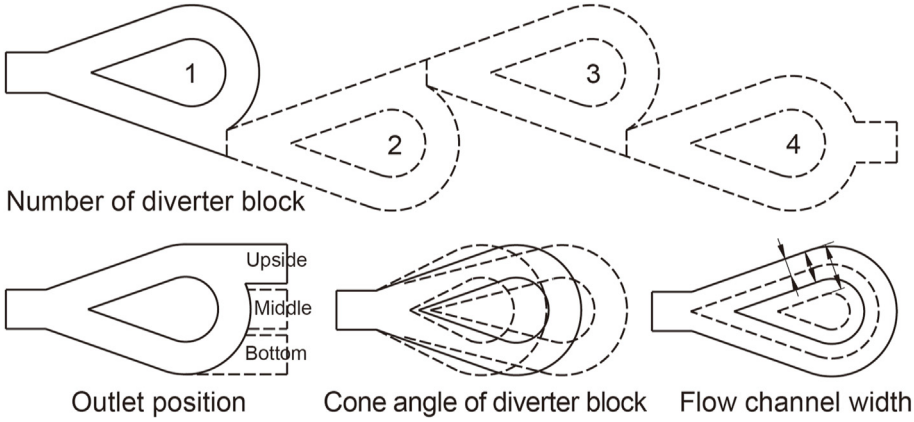

Fig. 12. Schematic diagram of composite type AICD's structural parameters.

can be observed that the flow paths of oil and water are significantly different, which also verifies that in the first section of the article, oil and water chose their respective flow paths due to different resistance. Fig. 14 shows the oil-water single-phase throttling pressure drop and oil-water two-phase volume fraction ratio corresponding to different outlet positions.

As can be seen from the above figure, as the outlet position moves from upside to bottom, the oil pressure drop hardly changes, and the water pressure drop significantly decreases. This is because the oil is mainly affected by the frictional drag and local pressure difference drag, and these drags has nothing to do with the outlet position. Water is mainly affected by the last diverter block, when the outlet is located on the maximum flow path (when the outlet is at the upper part, the flow path of water is the longest), the water flow direction changes severely in the last diverter block area, resulting in the strongest vortex and the maximum vortex drag. As the outlet position moves down, the effect of the vortex current will be weakened, and the vortex drag will decrease.

4.2. Number of diverter blocks

Limited by the structure size, the number of diverter blocks should not exceed 6. Fig. 15 shows the corresponding velocity contours of oil and water with different numbers of diverter blocks. Oil and water still maintain their respective flow paths as the number of diverter blocks increases. Fig. 16 shows the oil-water single-phase throttling pressure drop and oil-water two-phase volume fraction ratio corresponding to different numbers of diverter blocks.

From the simulation calculation results, it can be seen that the pressure drop of oil and water is sensitive to the number of guide blocks, the pressure drop of oil and water is directly proportional to the number of guide blocks, and the differential pressure drag of water and the friction drag of oil increase significantly. The increase of the throttling pressure drop in the water phase is greater than that of the oil, which indicates that the increase in the number of diversion blocks has a stronger restricted effect on water. When number of diverters is 5, it exhibits highest oil/water volume ratio which indicates the best water restricted effect.

4.3. Diverter block cone angle

Fig. 17 is the velocity contours of oil and water corresponding to different cone angles of the diverter block. It can be seen from the figure that as the angle of the cone surface increases, the diverter block becomes more “rounded” from “slender”, and the total length of the model also decreases. Fig. 18 shows the oil-water single-phase throttling pressure drop and oil-water two-phase volume fraction ratio corresponding to different cone angles of the diverter block.

It can be seen from Fig. 18 that with the increase of the cone angle of the diverter block, the throttling pressure drop of the oil phase shows a downward trend as a whole, while the water phase increases gradually. This is because the angle of the conical surface of the diverter block increases while the radius does not change, which reduces the length of the entire model, resulting in a shortened flow path and reduced frictional drag to the oil. At the same time, the upstream surface of the diverter block becomes more “blunt”, and the direction of water flow changes more violently, the vortices generated at the tail of each diverter block are also stronger, the vortex drag of the water increases, which enhances the hindering effect on the water. When the cone angle is 50°, it exhibits highest oil/water volume ratio which indicates the best water restricted effect.

4.4. Flow channel width

Fig. 19 shows the oil and water velocity contours for different flow channel widths. It can be seen from the figure that with the increase of the channel width, the volume of the diverter block is significantly reduced. Fig. 20 shows the pressure drop and volume fraction ratio of oil and water corresponding to different channel widths.

Increasing the width of the flow channel means that the volume of the diverter block decreases, and the distance between the outer

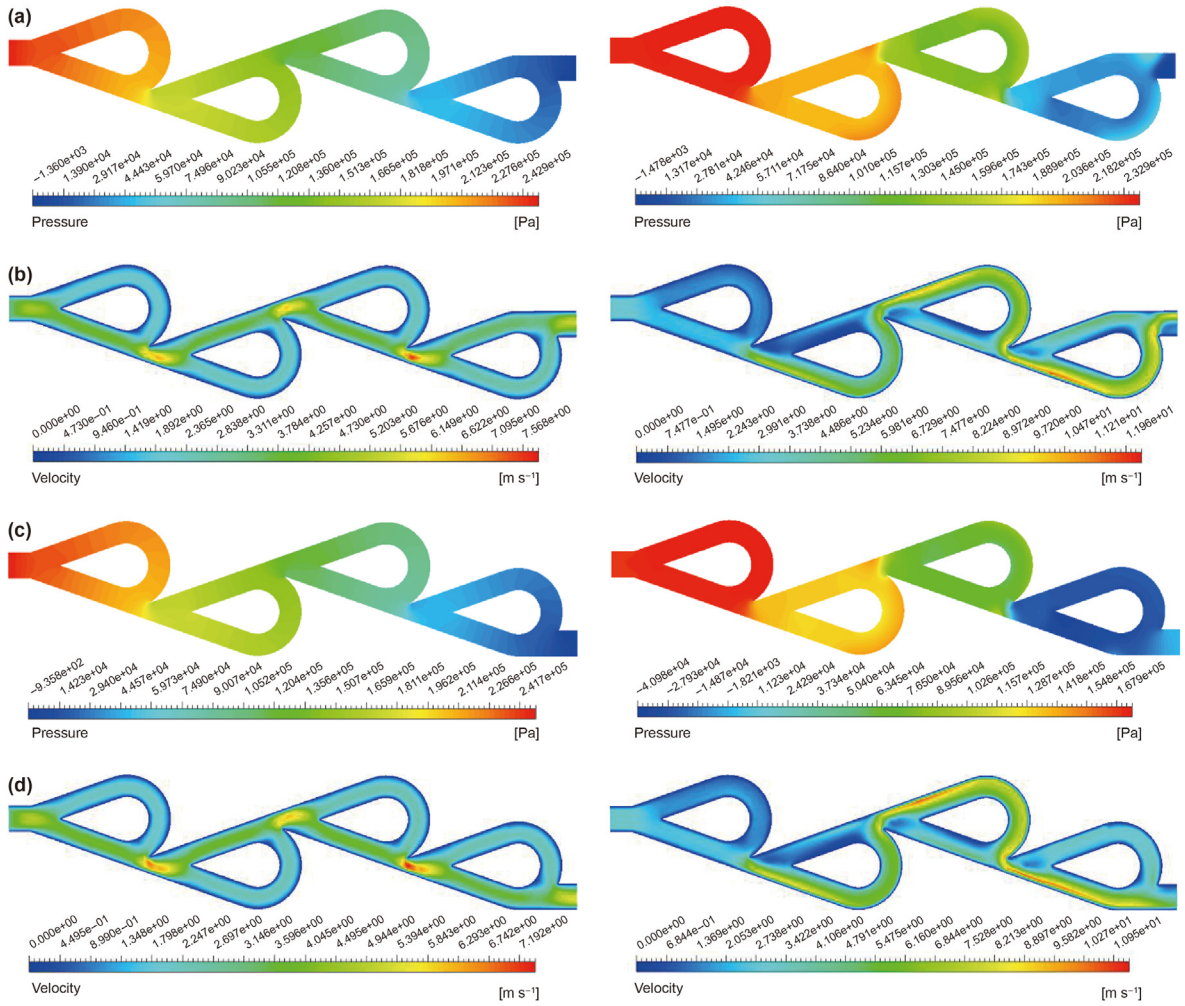

Fig. 13. Pressure contours and velocity contours corresponding to different outlet positions. (**a**) Oil (left) and water (right) pressure contours corresponding to the upside outlet position. (**b**) Oil (left) and water (right) velocity contours corresponding to the upside outlet position. (**c**) Oil (left) and water (right) pressure contours corresponding to the bottom outlet position. (**d**) Oil (left) and water (right) velocity contours corresponding to the bottom outlet position.

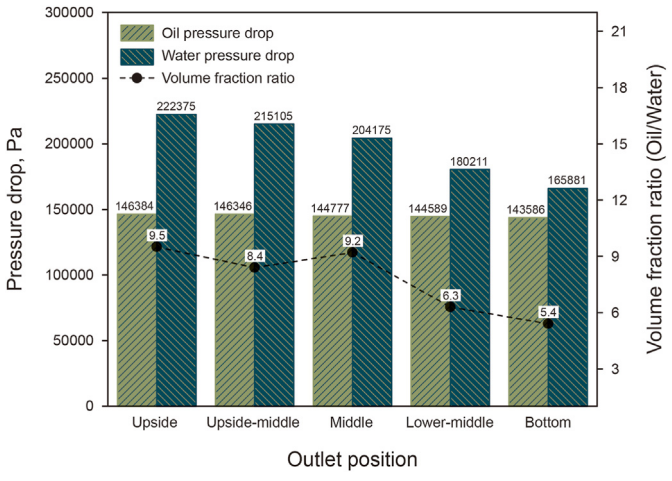

Fig. 14. Pressure drop and volume fraction ratio corresponding to different outlet positions.

wall of the diverter block and the inner wall of the flow channel is greater. At this time, the contact area between the oil and the diverter block is significantly reduced, and the frictional drag received is also greatly reduced, resulting in a decrease in oil pressure drop. As the volume of the diverter block decreases, the vortex generated by the water at the tail of the diverter block also weaken, and the vortex drag is also decreases, resulting in a decrease in water pressure drop. When the channel width is 2.5 mm, it exhibits highest oil/water volume ratio which indicates the best water restricted effect.

5. Comparative analysis of water control performance

From the sensitivity analysis results, it can be seen that the composite water control device would have the best water control performance when it has a maximum flow path and with 5 diverter blocks, 50° cone angle and 2.5 mm channel width. This chapter will quote a common spiral-flow type AICD[17] structure, then compare it with the performance of this composite type AICD under different

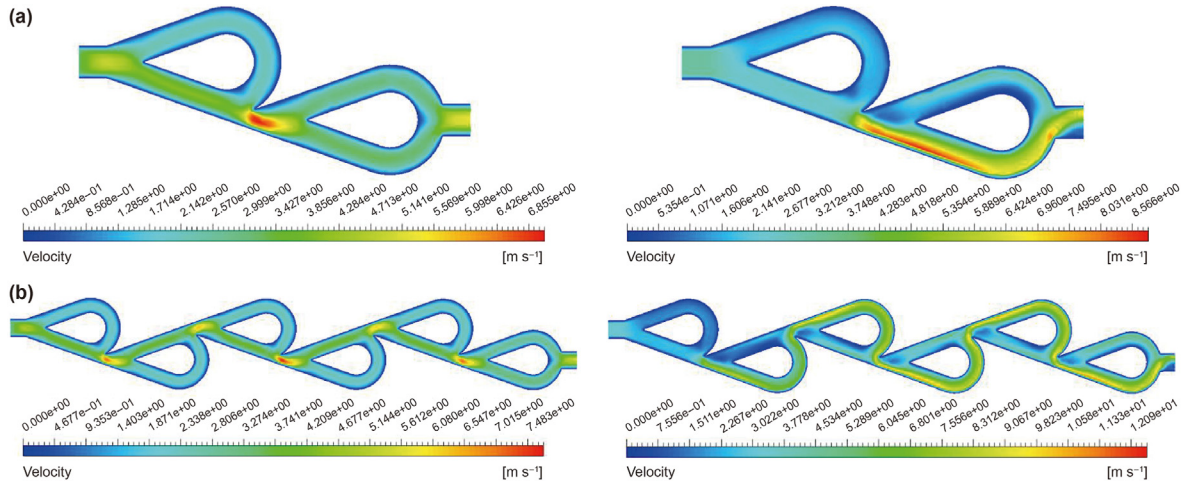

Fig. 15. Velocity contours corresponding to different number of diverter blocks. (**a**) Velocity contours of oil (left) and water (right) corresponding to the 2 diversion blocks. (**b**) Velocity contours of oil (left) and water (right) corresponding to the 6 diversion blocks.

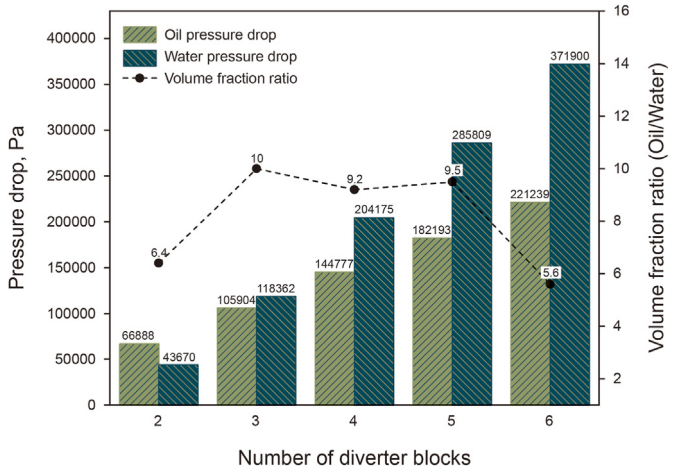

Fig. 16. Pressure drop and volume fraction ratio corresponding to different number of diverter blocks.

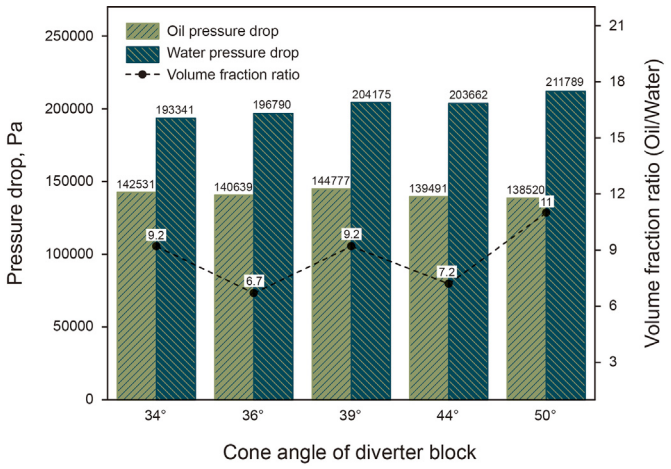

Fig. 18. Pressure drop and volume fraction ratio corresponding to different cone angle of diverter block.

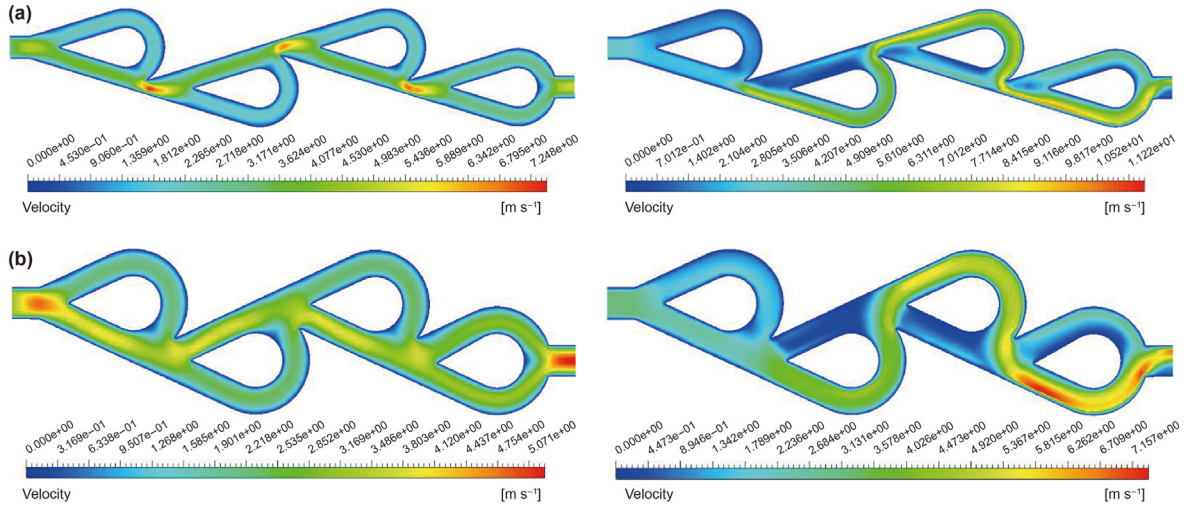

Fig. 17. Velocity contours corresponding to different cone angle of diverter block. (**a**) Velocity contours of oil (left) and water (right) corresponding to a 34° cone angle. (**b**) Velocity contours of oil (left) and water (right) corresponding to a 50° cone angle.

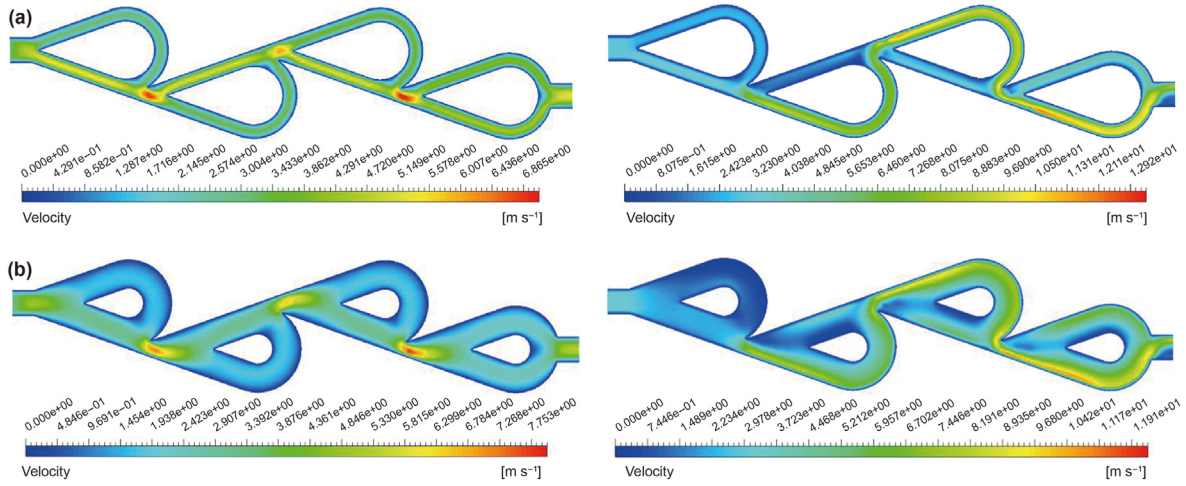

Fig. 19. Velocity contours corresponding to different flow channel width. (**a**) Velocity contours of oil (left) and water (right) corresponding to a flow channel width of 2 mm. (**b**) Velocity contours of oil (left) and water (right) corresponding to a flow channel width of 4 mm.

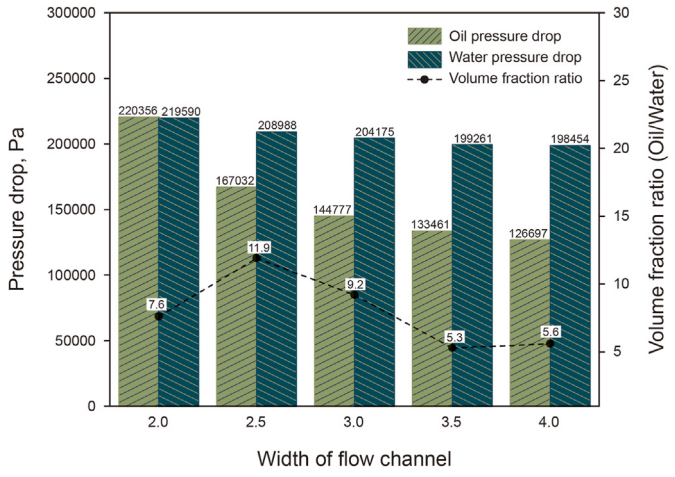

Fig. 20. Pressure drop and volume fraction ratio corresponding to different flow channel width.

fluid properties. As shown in Fig. 21, the optimized structure of this paper is shown by model A, and the comparison structure is shown by model B, the structural parameters of model A and model B are shown in Table 6. Table 7 shows the three fluid property scenarios of the sensitivity study in this paper.

5.1. Influence of water content on water restricted effect

The relationship between throttling pressure drop and water content is shown in Fig. 22. It can be seen from the figure that the pure water pressure drop of model A is four times that of model B, this means that the model A can generate greater resistance to water. From the slope chart in the figure, it can be seen that the sensitivity slope of model A starts to increase at a moisture content of 20%, while the sensitivity slope of model B only starts to increase at a moisture content of 70%. This indicates that model A is much more sensitive to moisture content than model B, and have significant limitations on water when the moisture content is low.

Fig. 21. Structure of model A (left) and model B (right).

Table 6
The structural parameters of Model A and Model B.

	Inlet area, mm^2	Outlet area, mm^2	Grid size, mm	Number of grids
Model A	10.5	10.5	0.3	59630
Model B	10.5	25π	0.5	54734

Table 7
Fluid properties study parameters.

	Water content, %	Oil density, kg/m^3	Oil viscosity, cp
Scheme 1	0, 10, 20, 30,40, 50, 60, 70, 80, 90, 100	850	100
Scheme 2	50	800, 850, 900, 950, 1000	100
Scheme 3	50	850	1, 5, 10, 20, 50, 100, 150, 200, 250, 300

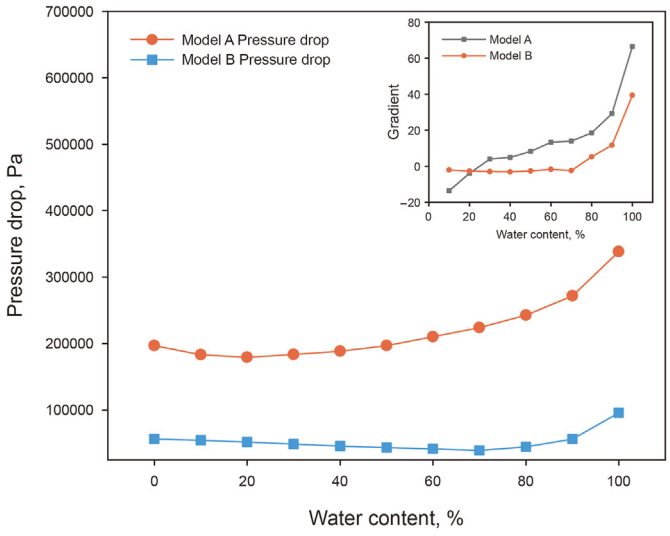

Fig. 22. Relationship curve between water content and pressure drop.

5.2. Influence of oil density on water restricted effect

The relationship between throttling pressure drop, volume fraction ratio and oil density is shown in Fig. 23(a). It can be seen from the figure that the throttling pressure drop and volume fraction ratio of model A are much greater than that of model B. The throttling pressure drop and volume fraction ratio of model B almost do not change with the increase of oil density, which shows that the model B is insensitive to the density. The throttling pressure drop of model A increases gradually with the increase of oil density, while the volume fraction ratio decreases greatly, which indicates that the water restricted effect is more sensitive to the density. The higher the density, the worse the water restricted effect of model A is. Fortunately, the density of the oil in the stratum is very stable, and there is no major change, so the model A can adapt to most of the stratum.

5.3. Influence of oil viscosity on water restricted effect

The relationship between throttling pressure drop, volume fraction ratio and oil viscosity is shown in Fig. 23(b). With the increase of oil viscosity, the throttling pressure drop of model A and model B decreased first and then increased, but the pressure drop of model A is much larger than that of model B. In this process, the flow state of the oil gradually changes from turbulent flow to laminar flow, and the frictional drag gradually increases. The oil-water volume fraction ratio of model B changes little, and is less sensitive to oil viscosity; the oil-water volume fraction ratio of model A decreases greatly with the increase of oil viscosity, and is more sensitive to viscosity, but still has good water restricted effect. Model A has a wide range of adaptation to viscosity, and can play a good role in controlling water and stabilizing oil for both light and heavy oil.

6. Conclusion

This paper proposes a multi-stage resistance-increasing composite type AICD which has been verified by experimental data. The performance of this AICD has been compared with that of an existing water control device. Results are summarized as below.

1. The composite type AICD has the water control effect of ICD and swirl type AICD at the same time, which can limit the rapid recovery of oil in the high permeability well section at the initial stage of production, thus balancing the production rate of each section of horizontal well and delaying the occurrence of bottom water coning; In the middle and later stages of production, water-blocking can be effectively increased to achieve water control and stable production.
2. A two-phase multistage separation resistance-increasing model was established, and the measurement experiments of throttling pressure drop and volume fraction were designed. Result indicates that the simulation result agrees qualitatively with that of the experimental data, verified the accuracy of the oil-

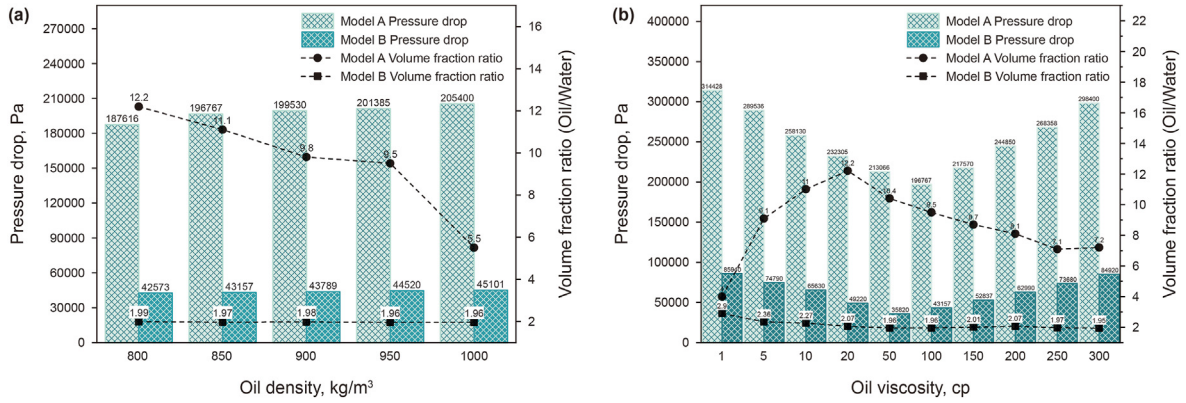

Fig. 23. Pressure drop and volume fraction ratio versus oil density and viscosity. (**a**) Relationship between oil density, throttling pressure drop, volume fraction ratio. (**b**) Relationship between oil viscosity, throttling pressure drop, volume fraction ratio.

water single-phase pressure drop simulation model and the oil-water two-phase volume fraction simulation model.

3. By analyzing the sensitivity of structural parameters, the sensitivity relationship between the pressure drop of oil and water and various structural parameters is obtained. The water pressure drop is more sensitive to the outlet position, number of diverter blocks, and cone angle of the diverter blocks of the composite AICD, while the oil pressure drop is more sensitive to the flow channel width of the composite AICD. The AICD has a greater impact on water pressure drop.
4. With the increase of water content, the water control ability of the composite type AICD is stronger. With the increase of oil density and viscosity, the water restricted effect of the AICD decreases, so it is not suitable for high density and high viscosity heavy oil.
5. The simulation calculation results show that, compared with the existing swirl type AICD like model B, composite AICD has higher sensitivity to moisture content, the water phase throttling pressure drop is increased by 4.5 times on average. The composite AICD is suitable for the entire stage of horizontal well production.

Conflict of interest

No potential conflict of interest was reported by the authors.

Acknowledgments

This research was supported by National Natural Science Foundation (52204050), Sichuan Science and Technology Program (2021ZHCG0013, 22ZDYF3009). The author thanks for their support and resources.

References

Al-Jumah, A., Gokmen, M., Harrasi, A., Abri, I., Buwaiqi, S., Urdaneta, G., 2022. Field Application of the Autonomous Inflow Control Device AICD for Optimized Heavy Oil Production in South Sultanate of Oman. SPE Conference at Oman Petroleum & Energy Show, Muscat, Oman. https://doi.org/10.2118/200279-MS.

Buwauqi, S., Jumah, A., Shabibi, A., Harrasi, A., Abd El-Fattah, M., Kalyani, T., Fahmy, A., 2022. Case Study: How the Newest Generation of Autonomous Inflow Control Device Helps to Control Excessive Wells Water Production within a Major Sultanate of oman Oilfield. Offshore Technology Conference Asia, Virtual and Kuala Lumpur, Malaysia. https://doi.org/10.4043/31483-MS.

Chen, D.Q., Zhao, H.W., Liu, K., Huang, Y.M., Li, B.F., 2021. The effect of emulsion and foam on anti-water coning during nitrogen foam injection in bottom-water reservoirs. J. Petrol. Sci. Eng. 196, 107766. https://doi.org/10.1016/j.petrol.2020.107766.

Cui, X.J., Li, Y., Li, H.T., Luo, H.W., Zhang, J.F., Liu, Q., 2020. A novel automatic inflow-regulating valve for water control in horizontal wells. ACS Omega 5 (43), 28056–28072. https://doi.org/10.1021/acsomega.0c03611.

Dikshit, A., Woiceshyn, G., Hanel, L., 2020. A systematic approach to the design and development of a new ICD to minimize erosion and erosion-corrosion. SPE Drill. Complet. 35 (3), 414–427. https://doi.org/10.2118/197601-PA.

Huang, X.T., Sun, P.N., Lv, H.G., Yin, X.R., Dong, J.X., 2022. Study on the viscous flow around foils with a multi-resolution smooth particle hydrodynamics method. J. Northwest. Polytech. Univ. 40 (3), 661–669. https://doi.org/10.1051/jnwpu/20224030661 (in Chinese).

Jia, P., Xue, S.F., Lei, Y.J., Zhu, X.X., Zhou, B., Wang, H.J., Zhu, Y., Fang, J., 2021. Water control performance and Structural parameter optimization of a floating disc adaptive inflow control device. Journal of China University of Petroleum 45 (5), 136–143. https://doi.org/10.3969/j.issn.1673-5005.2021.05.016 (in Chinese).

Jie, Y.N., Yang, J., Zhou, D.S., Wang, H.Y., Zou, Y., Liu, Y.F., Zhang, Y.J., 2022. Study on the optimal volume fracturing design for horizontal wells in tight oil reservoirs. Sustainability 14 (23), 15531. https://doi.org/10.3390/su142315531.

Langaas, K., Jeurissen, E., Abay, K., 2019. Combining passive and autonomous inflow-control devices in a trilateral horizontal well in the Alvheim Field. SPE Prod. Oper. 34 (3), 446–460. https://doi.org/10.2118/187288-PA.

Liu, J.L., Liang, X.L., 2022. Experimental study on frictional pressure drop of two-phase flow in mini-channel. Chem. Eng. 50 (1), 41–46 (in Chinese).

Mahmood, M., Guo, B.Y., 2021. Productivity comparison of radial lateral wells and horizontal snake wells applied to marine gas hydrate reservoir development. Petroleum 7 (4), 407–413. https://doi.org/10.1016/j.petlm.2021.10.004.

Pinilla, A., Stanko, M., Asuaje, M., Ratkovich, N., 2022. In-depth understanding of ICD completion technology working principle. Processes 10 (8), 1493. https://doi.org/10.3390/pr10081493.

Prakasa, B., Muradov, K., Davies, D., 2019. Principles of rapid design of an inflow control device completion in homogeneous and heterogeneous reservoirs using type curves. J. Petrol. Sci. Eng. 176, 862–879. https://doi.org/10.1016/j.petrol.2019.01.104.

Sabet, N., Irani, M., Hassanzadeh, H., 2022. Inflow control devices placement: a computational fluid dynamics approach. SPE J. 27 (3), 1562–1576. https://doi.org/10.2118/209211-PA.

Simonds, F, Zhao, L, Montoya, J., 2023. Novel inflow control device bridges the gap between passive and autonomous technologies. SPE Canadian Energy Technology Conference. https://doi.org/10.2118/212775-MS.

Toshev, S., Rakhimov, B., 2022. Well production increased when drilling horizontal wells. J. Phys.: Conference Series. IOP Publishing 2388 (1), 12171. https://doi.org/10.1088/1742-6596/2388/1/012171.

Wang, X.Q., Wang, Z.M., Zeng, Q.S., 2014. A Novel Autonomous Inflow Control Device: Design, Stracture Optimization, and Fluid Sensitivity Analysis. International Petroleum Technology Conference. IPTC, IPTC-17758-MS. https://doi.org/10.2523/IPTC-17758-MS.

Xu, N., Jiang, X.X., Yuan, R., Feng, W., 2019. Experimental study on frictional pressure drop of oil-water two-phase flow in rectangular microchannels. Journal of Central North University: Natural Science Edition 40 (1), 44–48. https://doi.org/10.3969/j.issn.1673-3193.2019.01.008 (in Chinese).

Yang, M.J., Wu, X.Y., Yue, Y.C., Zhang, Y., Chen, Y., Tang, Y.F., 2020. Design and analysis of a new profile control tool: swirling autonomous inflow-control device. SPE Prod. Oper. 35 (2), 351–361. https://doi.org/10.2118/199364-PA.

Yao, X., Xu, L., Wang, C., Ding, B., Zhao, L., 2023. Operational theory and qualification of a unique autonomous inflow control device for first use in a heavy oil layered reservoir. SPE Western Regional Meeting. https://doi.org/10.2118/214513-MS.

Zhang, N., Li, H.T., Liu, Y.G., Shan, J.C., Tan, Y.S., Li, Y., 2019. A new autonomous inflow control device designed for a loose sand oil reservoir with bottom water. J. Petrol. Sci. Eng. 178, 344–355. https://doi.org/10.1016/j.petrol.2019.03.034.

Zhang, R., Zhang, Z.Z., Li, Z., Jia, Z.Y., Yang, B., Zhang, J.P., Zhang, C., Zhang, G.C., Yu, S.H., 2021. A multi-objective optimization method of inflow control device configuration. J. Petrol. Sci. Eng. 205, 108855. https://doi.org/10.1016/j.petrol.2021.108855.

Zhu, Y.H., Liao, Y., Chen, W.H., Luo, Q.Y., Sun, W., 2019. Evaluation method comparison and study of application effect of ICD technique in eastern oilfield in south China sea. Petroleum Geology and Engineering 33 (4), 76–79 (in Chinese).